



# Subduction controls the distribution and fragmentation of Earth's tectonic plates

Claire Mallard, Nicolas Coltice, Maria Seton, R.D. Müller, Paul J. Tackley

## ► To cite this version:

Claire Mallard, Nicolas Coltice, Maria Seton, R.D. Müller, Paul J. Tackley. Subduction controls the distribution and fragmentation of Earth's tectonic plates. *Nature*, Nature Publishing Group, 2016, 535 (7610), pp.140-143. <10.1038/nature17992>. <hal-01355818>

**HAL Id: hal-01355818**

**<https://hal.archives-ouvertes.fr/hal-01355818>**

Submitted on 24 Aug 2016

**HAL** is a multi-disciplinary open access archive for the deposit and dissemination of scientific research documents, whether they are published or not. The documents may come from teaching and research institutions in France or abroad, or from public or private research centers.

L'archive ouverte pluridisciplinaire **HAL**, est destinée au dépôt et à la diffusion de documents scientifiques de niveau recherche, publiés ou non, émanant des établissements d'enseignement et de recherche français ou étrangers, des laboratoires publics ou privés.

# **Subduction controls the distribution and fragmentation of Earth's tectonic plates**

Claire Mallard<sup>1</sup>, Nicolas Coltice<sup>1,2</sup>, Maria Seton<sup>3</sup>, R. Dietmar Müller<sup>3</sup>, Paul J. Tackley<sup>4</sup>

1. Laboratoire de géologie de Lyon, École Normale Supérieure, Université de Lyon 1, 69622 Villeurbanne, France.

2. Institut Universitaire de France, 103, Bd Saint Michel, 75005 Paris, France

3. EarthByte Group, School of Geosciences, Madsen Building F09, University of Sydney, NSW, 2006, Australia

4. Institute of Geophysics, Department of Earth Sciences, ETH Zürich, Sonneggstrasse 5, 8092 Zurich, Switzerland



**The theory of plate tectonics describes how the surface of the Earth is split into an organized jigsaw of seven large plates<sup>1</sup> of similar sizes and a population of smaller plates, whose areas follow a fractal distribution<sup>2,3</sup>. The reconstruction of global tectonics during the past 200 My<sup>4</sup> suggests that this layout is probably a long-term feature of our planet, but the forces governing it are unknown. Previous studies<sup>3,5,6</sup>, primarily based on statistical properties of plate distributions, were unable to resolve how the size of plates is determined by lithosphere properties and/or underlying mantle convection. Here, we demonstrate that the plate layout of the Earth is produced by a dynamic feedback between mantle convection and the strength of the lithosphere. Using 3D spherical models of mantle convection with plate-like behaviour that match the plate size-frequency distribution observed for Earth, we show that subduction geometry drives the tectonic fragmentation that generates plates. The spacing between slabs controls the layout of large plates, and the stresses caused by the bending of trenches, break plates into smaller fragments. Our results explain why the fast evolution in small back-arc plates<sup>7,8</sup> reflects the dramatic changes in plate motions during times of major reorganizations. Our study opens the way to use convection simulations with plate-like behaviour to unravel how global tectonics and mantle convection are dynamically connected.**

The outer shell of our planet is comprised of an interlocking mosaic of 52 tectonic plates<sup>2</sup>. Among these plates, two groups are distinguished: a group of large plates with 7 plates of similar area

covering up to 94% of the planet, and a group of smaller plates, whose areas follow a fractal distribution<sup>2,3</sup>. The presence of these two statistically distinct groups was previously proposed to reflect two distinct evolutionary laws: the large plate group being tied to mantle flow and the other to lithosphere dynamics<sup>3</sup>. In contrast, others studies<sup>5,6</sup> have suggested that the plate layout is produced by superficial processes, because the larger plates may also fit a fractal distribution. Resolving this controversy has been limited by the exclusive use of statistical tools, which do not provide an understanding of the underlying forces and physical principles behind the organization of the plate system.

Here, for the first time, we use 3D spherical models of mantle convection to uncover the geodynamical processes driving the tessellation of tectonic plates. Our dynamic models combine pseudo-plasticity and large lateral and depth viscosity variations (Fig. 1; see Methods), which generate a plate-like behaviour self-consistently<sup>9,10,11</sup>, including fundamental features of seafloor spreading<sup>12</sup>. In our models, pseudo-plasticity is implemented through a yield stress that represents a plastic limit where the viscosity drops and strain localization occurs, producing the equivalent of plate boundaries. The value of the yield stress is a measure of the stress at plate boundaries and is not an experimental value. We determine the yield stress range that allows plate-like behaviour, as in previous studies<sup>13,14,15</sup>. For our convection parameterization, this range exists between 100 MPa, below which surface deformation is very diffuse, and 350 MPa, over which the surface consists of a stagnant lid. We analyse the plate pattern of models with yield stresses of 100 MPa (model 1), 150 MPa (model 2), 200 MPa (model 3) and 250 MPa (model 4) (see Fig. 1). Typically, 90% of the deformation is concentrated in less than 15% of the surface in our models.

Convection modelling generates continuous fields. As a consequence, we have to use plate tectonics rules to delineate the layouts of plates that self-consistently emerge in our dynamical solutions. We digitise plate boundaries on several snapshots for each yield stress value. To be sure that we study snapshots that are significantly different and not correlated with each other, we pick snapshots separated by more than 100 Myr<sup>16</sup>. We study 3 snapshots for model 1, and 5 snapshots for every other models (see Methods). We manually build plate polygons using GPlates<sup>17</sup> through a careful analysis of the surface velocity, horizontal divergence, viscosity, synthetic seafloor age, and

temperature field for each snapshot (see Methods, Extended Data Fig. 1 and 2). Thereby, we extract the cumulative number versus area distribution of plates for each convection snapshot (Fig. 2).

In model 1 (Fig. 2a), there are more than a hundred plates distributed along a smooth curve. The smallest plate has a size similar to the Easter microplate, and the largest one is smaller than the South American plate, which is significantly smaller than Earth's larger plates. In contrast, for model 4, the largest plate is larger than the Pacific plate, and small plates are absent (Fig. 2d). The snapshots of models with intermediate yield stresses (model 2 and 3) display the same two distributions of plate sizes observed on Earth (Fig. 2b; c, Extended Data Fig. 3). For a yield stress of 150 MPa (Fig. 2b), the smallest plate is the equivalent of the South Sandwich microplate, and the size of the largest one is between the area of the North American plate and the Pacific plate. For a yield stress of 200 MPa (Fig. 2d), the smallest plate is slightly larger than that for a yield stress of 150 MPa, but the largest plate is close in area to the Pacific plate.

Our models indicate that the maximum plate size increases with increasing yield stress, which itself has also the effect of increasing the wavelength of convection<sup>15</sup>. For the lowest yield stress value, the spherical harmonic power spectrum of the temperature field is dominated by shorter wavelengths, and by degree 6 in the shallow boundary layer (Fig. 1f), representing the existence of numerous subduction zones and relatively short wavelengths of the flow in the mantle. For the two intermediate values of 150 MPa and 200 MPa (Fig. 1g-h), the spectra drift to larger wavelength since degree 4 dominates in the shallow boundary layer, corresponding to a lower number of subduction zones, and the maximum size of plates is similar in both cases. When the yield stress increases to 250 MPa (Fig. 1i) degree 2 dominates in the shallow boundary layer, corresponding to the maximum size of plates over all models. These results suggest that the size of the large plates follows the spacing between active downwellings.

Former studies on the distribution of smaller plates point to a fragmentation process<sup>5</sup>. We then focus on triple junctions, which are symptoms of plate fragmentation: the splitting of a plate into two smaller ones necessarily produces two triple junctions. Both models and Earth display significantly more triple junctions on subduction zones than on mid-ocean ridges (106.6 vs. 75.6 on average for model 2; 131

vs. 71 on Earth today), despite the fact that mid-ocean ridges are more elongated than trenches (total length of mid-ocean ridges and transform: 79,000 km vs 66,000 km on average for model 2; 72,500 km vs 48,000 km on Earth today). Likewise, the triple junctions mainly composed of trench segments are those involving smaller plates in higher proportions (Extended Data Fig. 4). Hence, subduction zones focus fragmentation and smaller plate formation. On Earth, only the Galapagos, Easter, and Juan Fernandez plates form away from any trench or collisional area.

Our calculations show plates fragments mostly in connection with curved trenches. Indeed, surface velocities tend to be perpendicular to the trench where slabs sink. Therefore a bend of the trench corresponds to differential motion hence high stresses. As a consequence, the concave plate under tensile stresses fragments and triple junctions connects the trench with new ridge/transform/diffuse segments. This is consistent with the observed correlation between the tortuosity of trenches and the number of triple junctions per unit length of subduction (Fig. 3). Because increasing the yield stress produces less tortuous trenches and fewer triple junctions per unit length of trench, smaller plate generation is also controlled by the strength of the lithosphere,.

The models we present with plate area distributions similar to Earth have lengths of convergent boundaries similar to our planet, when comparing trenches in our models with trenches plus mountain belts on Earth<sup>2</sup>. Moreover, the computed temperature heterogeneity spectra of the intermediate yield stress case (Fig. 1 g) have a degree 2 dominating in the deep mantle, consistent with tomographic models of the Earth's mantle<sup>18</sup>(Fig. 1 j). However, our models include simplifications because of computational limitations: a lower Rayleigh number than on Earth ( $10^6$  vs.  $\sim 10^7$ ), incompressibility, no chemical differences (no continents, no deep chemical piles). The physics principles we propose for the plate size distribution are not specifically dependent on the Rayleigh number<sup>19</sup>, although the values of the yield stress could be different. Compressibility should have little impact on the surface tectonics since it concerns the deeper flow<sup>20</sup>. The addition of continents which help generate more Earth-like area-age distributions of the seafloor<sup>12</sup>, should reinforce the presence of the larger plates and ensure large-scale flow.

Based on our results, we propose that the plate pattern on Earth is produced by the dynamic feedback between mantle convection and the strength of the lithosphere. The self-organised subduction structure defines the pattern of large and small plates through slab pull and suction. The large plates system evolves over 100s of My through global reorganisations of mantle flow due to initiation and shutdown of subduction (Fig 4.). This timescale is commensurate with the lifetime of slabs<sup>21</sup>. In contrast, the smaller plates in our models evolve on shorter timescales of 10s of My (Fig. 4). They record lateral changes in trench geometry and slab migrations<sup>22</sup>. The enhanced sensitivity of the smaller plates to readjustment of subduction systems is consistent with present-day observations of seafloor spreading in many back-arc regions. They reveal that global and regional changes in plate motions may be more readily and dramatically expressed in these smaller plates than in the larger plates. For instance, the Parece Vela and Shikoku Basins in the Philippine Sea plate record a major clockwise change in spreading direction between 22-23 Ma<sup>7</sup>, at the same time that the larger Pacific plate records significant plate boundary and plate motion changes (e.g. the fragmentation of the Farallon plate<sup>23</sup>, collision of Ontong Java Plateau with the Melanesian subduction zone<sup>24</sup>). In the same way, the Lau Basin in the SW Pacific initiated its main spreading phase by successive southward propagation around 4 Ma<sup>8</sup>, at the same time as a change in spreading direction in the northeast<sup>25</sup> and southwest Pacific<sup>26</sup> and a major phase of subsidence across the Atlantic<sup>27</sup>.

We propose that the plate layout is a property characterizing a dynamic feedback between mantle convection and lithosphere strength. The larger plates are an expression of the dominating convection wavelength, and their fragmentation into smaller plates is driven by subduction geometry. Therefore, the decreasing number of smaller plates in pre-Cenozoic tectonic reconstructions<sup>3,4</sup> is an artificial consequence of the diminishing quantity of preserved seafloor. Confirming the existence of migrating intra-oceanic subduction systems like in Panthalassa<sup>28</sup>, may help correct that bias. Over longer geologic time scales, the size distribution of plates has certainly evolved in relationship with the slow cooling of the Earth. Following the weakening of convective vigor, the lithosphere gets stronger relative to mantle forces. Therefore, this study suggests that since plate tectonics started on Earth, it may have operated with less but larger plates as the planet has cooled down.

**Acknowledgements** The research leading to these results was funded by the European Research Council within the framework of the SP2-Ideas Programme ERC-2013-CoG under ERC grant agreement 617588. We thank S. Durand and E. Debayle for helping to make Fig. 1e, i and E. J. Garnero for his inputs. Calculations were performed on the AUGURY supercomputer at P2CHPD Lyon. N.C. was supported by the Institut Universitaire de France. R.D.M and M.S are supported by ARC grants DP130101946 and FT130101564.

## References

1. Le Pichon, X. Sea-Floor spreading and continental drift. *J. Geophys. Res.* **73** (12), 3661–3697 (1968).
2. Bird, P. An updated digital model of plate boundaries. *Geochem. Geophys. Geosys.* **4**, 1027 (2003).
3. Morra, G., Seton, M., Quevedo, L. & Müller, R. D. Organization of the tectonic plates in the last 200Myr. *Earth Planet. Sci. Lett.* **373**, 93–101 (2013).
4. Seton, M., Müller, R.D., Zahirovic, S., Gaina, C., Torsvik, T., Shephard, G., Talsma, A., Gurnis, M., Turner, M., Maus, S. & Chandler, M. Global continental and ocean basin reconstructions since 200Ma, *Earth Sci. Rev.* **113**, 212–270 (2012).
5. Sornette, D. & Pisarenko, V. Fractal Plate Tectonics. *Geophys. Res. Lett.* **30**, 1105 (2003).
6. Vallianatos, F. & Sammonds, P. Is plate tectonics a case of non-extensive thermodynamics ? *Physica A*, **389**, 4989–4993 (2010).
7. Sdrolias, M., Roest, W. R. & Müller, R. D. An expression of Philippine Sea plate rotation: the Parece Vela and Shikoku Basins. *Tectonophysics*. **394**, 69–86 (2004).
8. Taylor, B., Zellmer, K., Martinez, F. & Goodliffe, A. Sea-floor spreading in the Lau back-arc basin. *Earth Planet. Sci. Lett.* **144**, 35-40 (1996)
9. Moresi, L. & Solomatov V. Mantle convection with a brittle lithosphere : thoughts on the global tectonic styles of the Earth and Venus. *Geophys. J. Int.* **133**, 669–682 (1998).
10. Trompert, R. & Hansen U. Mantle convection simulations with rheologies that generate plate-like behaviour. *Nature*. **395**, 686–689 (1998).
11. Tackley, P. J. Self-consistent generation of tectonic plates in time-dependent, three dimensional mantle convection simulations : 1. Pseudoplastic yielding. *Geochemistry, Geophys. Geosystems*. **1** (2000a).
12. Coltice, N., Seton, M., Rolf, T., Müller, R., & Tackley P. J. Convergence of tectonic reconstructions and mantle convection models for significant fluctuations in seafloor spreading. *Earth Planet. Sci. Lett.* **383**, 92–100 (2013).
13. Ricard, Y., Bercovici, D. & Schubert. G. A two-phase model for compaction and damage : 2. Applications to compaction, deformation, and the role of interfacial surface tension. *J. Geophys. Res.* **106**, 8907 (2001).
14. Stein, C., Schmalz, J. & Hansen, U. The effect of rheological parameters on plate behaviour in a self-consistent model of mantle convection. *Phys. Earth Planet. Inter.* **142**, 225–255 (2004).

15. Van Heck, H. J. & Tackley, P. J. Planforms of self-consistently generated plates in 3D spherical geometry. *Geophysical Research Letters*. **35**, L19312 (2008).
16. Bello, L., Coltice, N., Rolf, T., & Tackley, P. J. On the predictability limit of convection models of the Earth's mantle. *Geochemistry, Geophysics, Geosystems*. **15**, 1–10. (2014).
17. Williams, S. E., Müller, R. D., & Landgrebe, T. C. W. An open-source software environment for visualizing and refining plate tectonic reconstructions using high-resolution geological and geophysical data sets. *GSA TODAY*. **22**, 4–9 (2012).
18. Becker, T. W. & Boschi, L. A comparison of tomographic and geodynamic mantle models. *Geochem., Geophys., Geosys.* **3**, 1003 (2002).
19. Van Heck, H. J., & Tackley, P. J. Plate tectonics on super-Earths: Equally or more likely than on Earth. *Earth Planet. Sci. Lett.* **310**, 252-261 (2011).
20. Tackley, P. J. Modelling compressible mantle convection with large viscosity contrasts in a three-dimensional spherical shell using the yin-yang grid. *Phys. Earth Planet. Inter.* **171**, 7–18 (2008).
21. Matthews, K.J., Seton, M., Müller, R.D. A global-scale plate reorganization event at 105-100 Ma. *Earth Planet. Sci. Lett.* , **355–356**, 283-298 (2012).
22. Stegman, D.R., Schellart, W.P., Freeman, J. Competing influences of plate width and far-field boundary conditions on trench migration and morphology of subducted slabs in the upper mantle. *Tectonophysics*. **483**, 46–57 (2010).
23. Barckhausen, U., Ranero, C.R., Cande, S.C., Engels, M. & Weinrebe, W. Birth of an intraoceanic spreading center. *Geology*. **36**, 767-770 (2008).
24. Petterson, M. G., Babbs, T., Neal, C. R., Mahoney, J. J., Saunders, A. D., Duncan, R. A., ... & Natogga, D. Geological–tectonic framework of Solomon Islands, SW Pacific: crustal accretion and growth within an intra-oceanic setting. *Tectonophysics*. **301**, 35-60 (1999).
25. Harbert, W. Late Neogene relative motions of the Pacific and North America plates. *Tectonics*. **10**, 1-15 (1991).
26. Tebbens, S., & Cande, S. Southeast Pacific tectonic evolution from early Oligocene. *J. geophys. Res.* **102**, 061-12 (1997).
27. Cloetingh, S. A. P. L., Gradstein, F. M., Kooi, H., Grant, A. C., & Kaminski, M. M. Plate reorganization: a cause of rapid late Neogene subsidence and sedimentation around the North Atlantic? *Journal of the Geological Society*. **147**, 495-506 (1990).
28. Van der Meer, D. G., Torsvik, T. H., Spakman, W., van Hinsbergen, D. J. J., & Amaru, M. L. Intra-Panthalassa Ocean subduction zones revealed by fossil arcs and mantle structure. *Nature Geoscience*. **5**, 215–219 (2012).
29. Amante, C. & Eakins, B.W. ETOPO1 1 Arc-Minute Global Relief Model: Procedures, Data Sources and Analysis. *US Department of Commerce, National Oceanic and Atmospheric Administration, National Environmental Satellite, Data, and Information Service, National Geophysical Data Center, Marine Geology and Geophysics Division*. 19pp (2009).
30. French, S. W. & Romanowicz, B. A. Broad plumes rooted at the base of the Earth's mantle beneath major hotspots. *Nature*. **525**, 95–99 (2015).



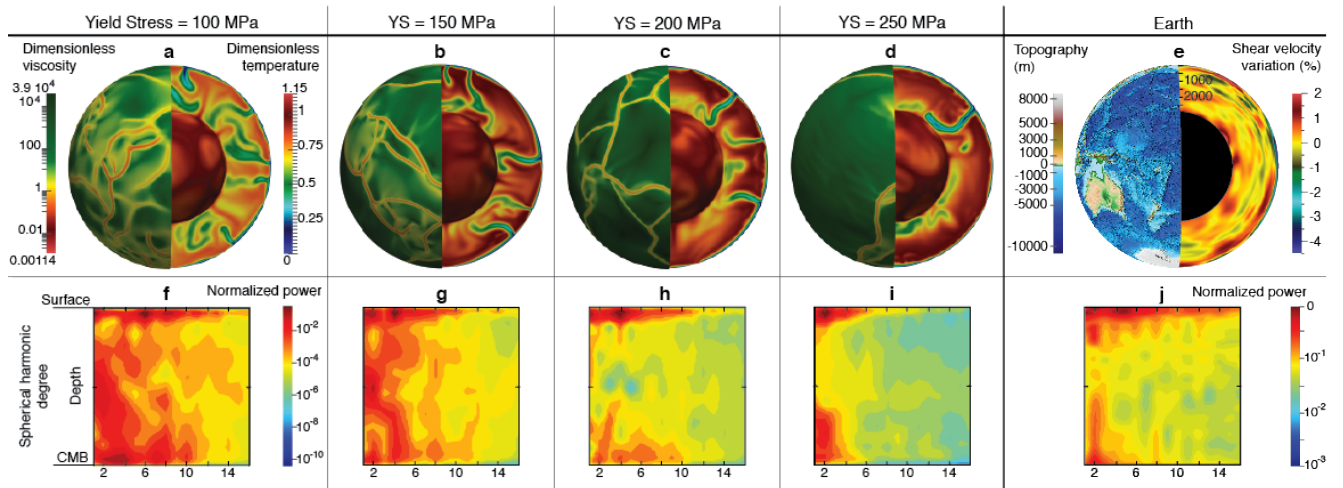


Figure 1 : Snapshots of convection calculations with four yield stress values (a-d) and of Earth today (e) with associated spectral heterogeneity maps of the temperature field (f-i) and seismic velocity field (j). The spectral heterogeneity maps are normalized by the value of the highest power. **a.** Convection solution with a yield stress = 100 MPa and containing a large number of plate boundaries. The spherical harmonic map **f.** is dominated by degree 6 in the shallow boundary layer. **b.** Convection solution with a yield stress = 150 MPa with fewer plate boundaries and a decreasing number of slabs. The spherical harmonic map **g.** is dominated by degree 4 at the surface. **c.** Convection solution with a yield stress = 200 MPa has even fewer plate boundaries. The spherical harmonic **h.** is dominated by degree 4 at the surface. **d.** Convection solution with a yield stress = 250 MPa has a barely deformed surface. The spherical harmonic map **i.** is blue and dominated by degree 2. **e.** ETOPO1<sup>29</sup> global relief model of the Earth and a cross section through S-wave tomographic model SEMUCB-WM1<sup>30</sup> centered on West America; the spherical harmonic map **j.** of the tomographic model is dominated by degree 4-5 at the surface.

Snapshots of convection calculations with four yield stress values and of Earth with associated spectral heterogeneity maps of the temperature field and seismic velocity field.

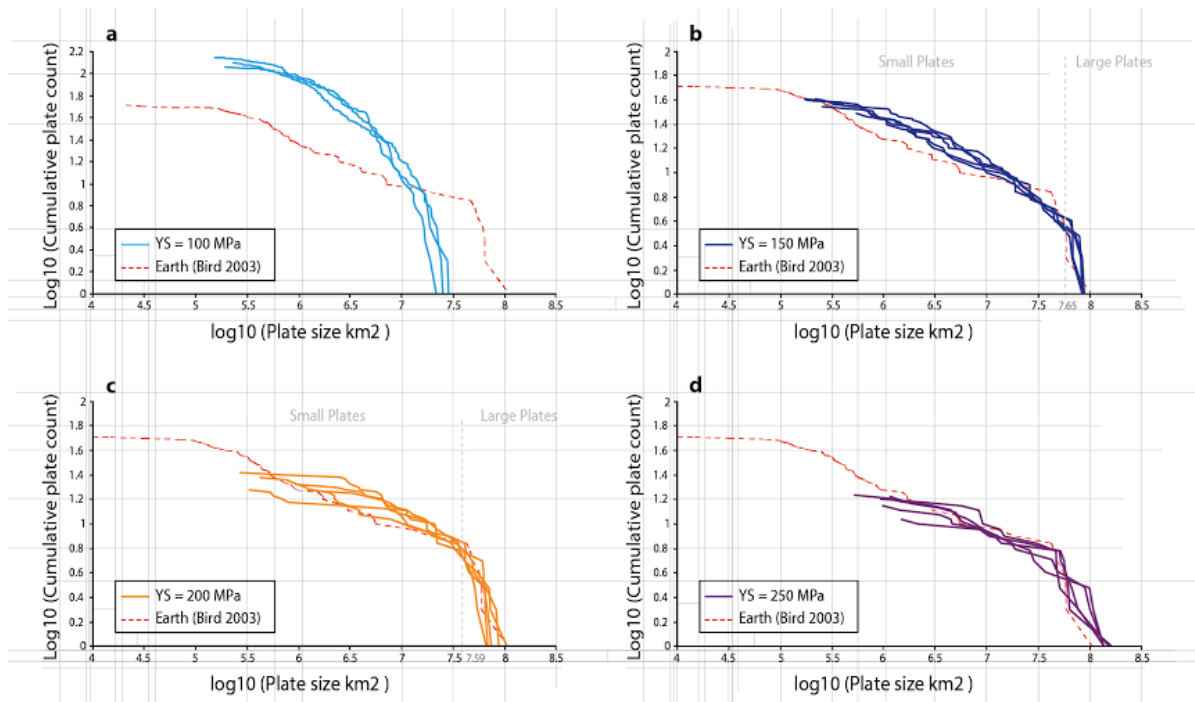


Figure 2 : Plot of the logarithm of cumulative plate count vs. the logarithm of plate size in  $\text{km}^2$  for four different yield stress values (YS) and the Earth. It represents the number of plates exceeding a given area. The graphs contain 3 datasets for YS = 100 MPa, 5 datasets for other yield stress values, and the dataset for the Earth<sup>2</sup> where the distinction between small plates and large plates is around 7.6 ( 39,800,000  $\text{km}^2$ ). **a.** Graph for models with yield stress of 100 MPa, showing a distribution of small and medium plates. **b.** Graph for models with yield stress of 150 MPa, showing a distinction between the large and the small plates distribution. The distribution changes at about 7.8 (63,100,000  $\text{km}^2$ ). **c.** Graph for model with yield stress of 200 MPa, displaying fewer small plates, the group of small and the group of large plates are distinct and split at about 7.6 (39,800,000  $\text{km}^2$ ). **d.** Graph for model with yield stress of 250 MPa, showing only medium and large plates. The division between smaller and large plates in b and c corresponds to the crossover of the fitted slopes of the large and smaller plates (Extended data Fig. 3) .

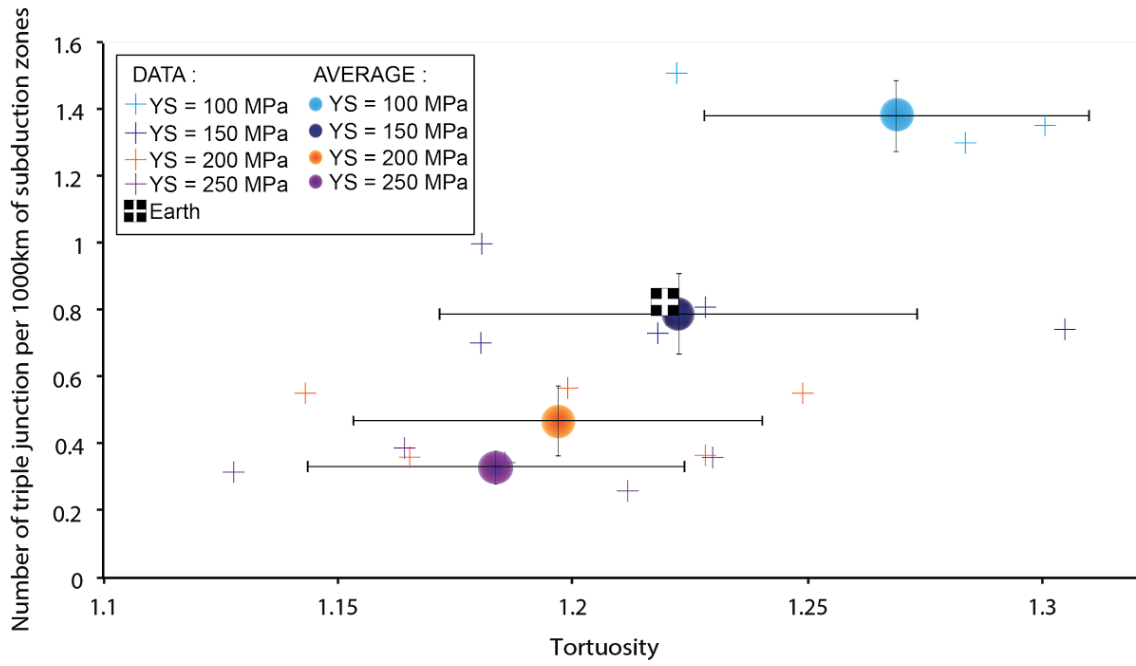


Figure 3 : Number of triple junctions per 1000 km of subduction zones vs. average tortuosity for the four models differing from their yield stress value (YS), and the Earth. The tortuosity is the ratio of the length of the subduction zone to the length of the great circle between the endpoints. The error bars represent the standard deviation for each data set.

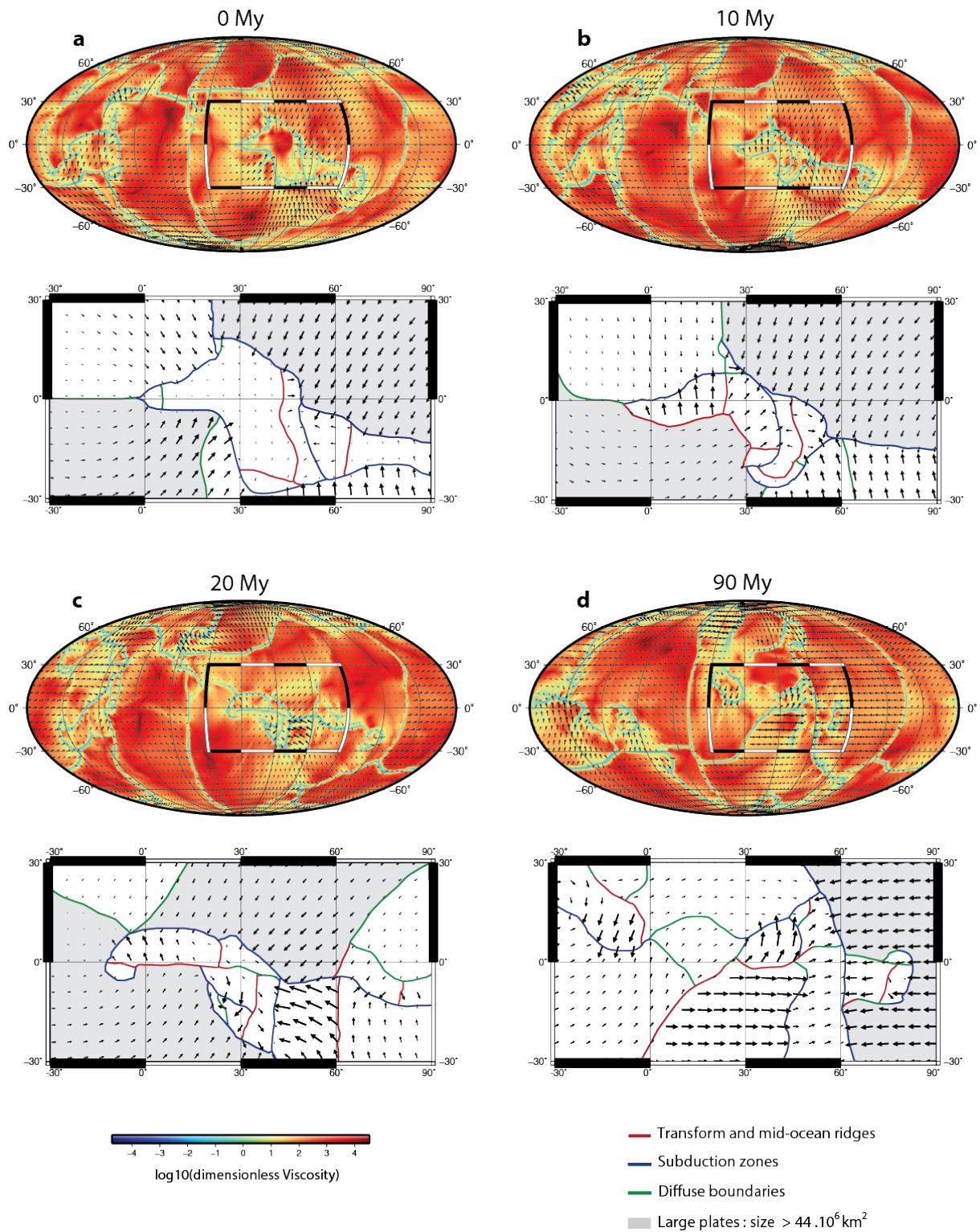


Figure 4 : Global viscosity maps of the model 2 and associated kinematics, with a focus on the area between  $-30^{\circ};90^{\circ}$  and  $30^{\circ};-30^{\circ}$ . **a**; **b**; **c** are separated by 10 Ma. The shape of large plates show very little changes, while the adjustment of small plates evolves quickly. **d**; 90My after the first snapshot, the distribution of large plates and smaller plates has evolved significantly. Plates in white are plates larger than  $45e6 \text{ km}^2$ , plates in medium grey have area between  $5.8e5$  and  $45e6 \text{ km}^2$ , and microplates are in dark grey. Plate categories are determined in Extended Data Fig. 3.

## Methods

### 1. Convection models

The models computed here have similar parameterizations to those published in Bello et al. (2015)<sup>31</sup>, except that no surface velocities are imposed here (free convection). We solve the non-dimensional equations of mass, momentum and heat conservation in 3D spherical geometry using the code StagYY<sup>32</sup>. The flow is incompressible under the Boussinesq approximation. Viscosity is the only variable material property in our models. Variations of other material properties (expansion coefficient, thermal diffusivity, heat production) are neglected.

The Rayleigh number  $Ra$  is defined here as

$$Ra = \frac{\rho g \alpha \Delta T L^3}{\kappa \eta_0}$$

where  $\rho$  is density,  $g$  the gravitational acceleration,  $\alpha$  the thermal expansivity,  $\Delta T$  the temperature drop across mantle depth,  $L$  the mantle thickness,  $\kappa$  is thermal diffusivity and  $\eta_0$  the reference viscosity at the base of the mantle. The non-dimensional temperature is set to  $T=0$  at the surface and  $T=1$  at the base of the mantle, and a non-dimensional internal heat production of 20 is chosen, such that the basal heat flux is about 14 % of the total. This is in the lower range of estimates for the heat flow at the core-mantle boundary<sup>33</sup>.

In our models,  $Ra$  is  $10^6$ , which is about 10-50 times lower than what is expected for the Earth, and produces a top boundary layer 300 km thick. We were limited to this Rayleigh number because of the computational power required to solve for convection with large viscosity variations. The average resolution is 45 km in laterally and vertically for all the models.

The viscosity in our models depends on temperature and depth as

$$\eta(T, z) = \eta_z(z) \exp\{0.064 + 30/(T + 1)\}$$

where  $z$  is the depth. The non-dimensional activation energy being 30 here produces 6 orders of magnitude of viscosity variations with temperature.

The depth-dependence of viscosity is taken into account such that

$$\eta_z(z) = a \exp\left\{\ln(B) \left[1 - 0.5 \left(1 - \tanh\left(\frac{d_0 - z}{d_{step}}\right)\right)\right]\right\}$$

where  $B$  stands for the factor of viscosity jump at depth  $d_0$  over a thickness  $2d_{step}$ , and  $a$  is a prefactor ensuring  $\eta_z = \eta_0$  for temperature  $T=1$  at the base of the mantle. Based on geoid<sup>34</sup> and post-glacial rebound<sup>35</sup>,  $B$  is set to 30 here and the jump of viscosity occurs between 750 km and 850 km deep ( $d_0$  is 0.276 and  $d_{step}$  is 0.02).

Pseudo-plasticity is implemented through a stress dependence of the viscosity with a yield stress<sup>36,37,38</sup>. When the local stress reaches the yield stress value  $\sigma_y$ , the viscosity is computed as

$$\eta = \frac{\sigma_y}{2\epsilon'}$$

where  $\epsilon'$  is the second invariant of the strain rate tensor. The StagYY code has been benchmarked with such rheology<sup>39</sup>. The yield stress is the only parameter varied in this study. Taking  $\eta_0 = 10^{23}$  Pa s, the values of the yield stress producing plate-like behaviour are between 100 MPa and 350 MPa.

In our models, the viscosity drops by a factor of 10 in the vicinity of ridges where the temperature crosses the solidus temperature given by a simple linear model  $T_{sol} = 0.6 + 7.5z$ , and without melt fraction dependence. This effect improves slightly plate-like behaviour and has been used in previous studies<sup>38,40</sup>.

The models are started from ad hoc initial conditions, and run for up to 5 billion years to ensure statistical steady-state and stability of the dynamic regime. Such long runs ensure that initial conditions are forgotten. From the solutions at statistical steady-state, we compute the dynamic evolutions of the models that are analyzed in this study.

## 2. Building tectonic plates

We established a method to define the boundaries and the geometry of tectonic plates on the surface of our convection models. At first, the boundaries need to be identified to define the outline of the plates themselves (plate polygons). The same method was applied for every of the 18 snapshots of models we present. This is a relatively small sample because the precise determination of the plate layout for 1 snapshot is very time-consuming. Only 3 snapshots have been studied for model 1 because of the large number of plates (more than 100). The GPlates software is used to trace all plate boundaries, interactively building digital plate tectonic layouts.

a. Identification of major boundaries

The first step is to identify the major and localized boundaries on the surface of the convection models. We use the viscosity, temperature and velocity data. The maps of seafloor ages obtained from the heat flux (Extended Data Fig. 1a), allow the youngest zones, at 0 Ma, to be identified as mid oceanic ridges and the oldest zones, from 180 to 280 Ma, as subduction zones. In the same manner, we use maps of the horizontal divergence (Extended Data Fig. 1b) inferred from the surface velocities. Hence, the divergence zones show the localization of the mid oceanic ridges for dimensionless divergence values of between 0 and 30,000 and the convergence zones, show the subduction zones with data of between -15,000 to 0. Transform zones (since our model is continuous, there are no faults but shear zones) exist in our models and are identified via surface vorticity maps. To minimize the time it takes to interactively build plate boundary models, the same group of boundaries includes mid-ocean ridges and transform zones. Nevertheless, for the model with a yield stress of 150 MPa we computed a length of mid-ocean ridges of about 79,000 km on average and a length of transform regions of about 2600 km. In comparison, these lengths on Earth are 67,000 km for mid-ocean ridges and 5131 km for transform regions.

The identification of these 2 types of major boundaries (subduction zones and mid-ocean ridges) does not always allow us to close polygons to obtain tectonic plates. Even if some boundaries can be extrapolated, many zones necessitate more thorough work as discussed below.

b. Identification of diffuse boundaries

To close polygons, other boundaries need to be defined. The study of deviatoric stress allows us to identify some diffuse junctions. In the models, non-yielded boundaries are set between two zones where the velocity vector is slightly changing. They exist in ductile zones, visible thanks to a fan of velocity vectors (Extended Data Fig. 2). This geometric configuration implies a large zone of deformation almost like intraplate deformation, which is defined as a diffuse boundary. That is exactly the definition of diffuse boundaries on Earth<sup>41</sup>. The delimitation of the diffuse boundaries between two zones with different velocity implies a non-negligible error in the estimation of the Euler pole (and the calculated velocities) we quantify.

The identification of these three types of boundaries (mid-oceanic ridges, subduction zones and diffuse boundary) allows us to close topological polygons defined by these boundaries (Extended Data Fig. 1c). These polygons are tectonic plates but before they can be used, we need to evaluate the error we made in the delimitation of tectonic plates according to the plate tectonic theory.

### c. Fit of the plate model with the convection model

We compare the raw velocity data of the convection models with the a posteriori velocities calculated using Euler's theorem for the corresponding plate layout. At first, we extract the raw velocity data for each plate using the plate polygons determined previously. We then use the raw velocities to invert for the angular velocity vector, using the inverse method described by Gourdazi (2014)<sup>42</sup>, and compute the predicted velocities based on the inverted angular velocity vector. As a measure of the quality of our plate model to fit the convection model, we compute the plateness  $P$  of the plate layout following Zhong et al.<sup>43</sup> :

$$P = 1 - \Delta V_{rms} / V_{rms},$$

where  $\Delta V_{rms}$  is the root mean square difference between the velocities of the convection model and those predicted with plate rotations, and  $V_{rms}$  is the root mean square surface velocity of the model. We obtain a plateness between 0.75 and 0.81 (1 would be perfectly rigid plates, 0 would absolutely preclude the use of plate approximation), which is consistent with the fact that 90% of the deformation is concentrated in 15% of the surface of the models.

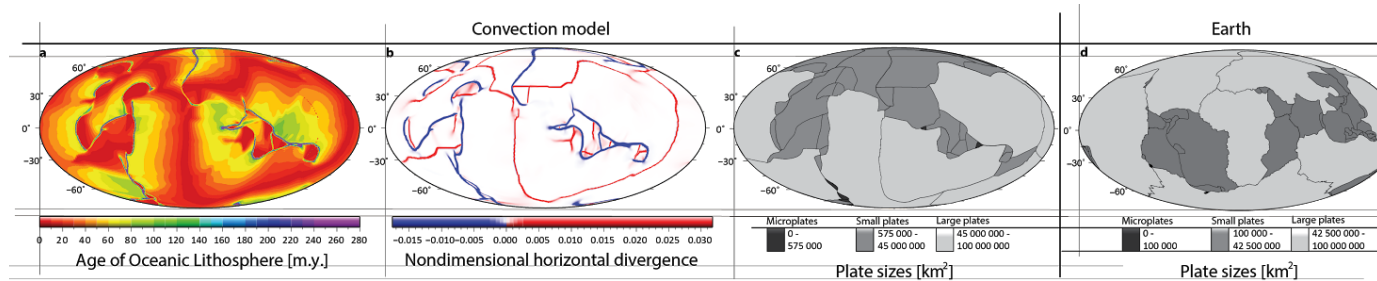
## References

31. Bello, L., Coltice, N., Rolf, T., & Tackley, P. J. On the predictability limit of convection models of the Earth's mantle. *Geochemistry, Geophysics, Geosystems*. **15**, 1–10 (2014).
32. Tackley, P. J. Modelling compressible mantle convection with large viscosity contrasts in a three-dimensional spherical shell using the yin-yang grid. *Phys. Earth Planet. Inter.* **171**, 7–18 (2008).
33. Lay, T., Hernlund, J., & Buffett, B. A. Core–mantle boundary heat flow. *Nature Geoscience*. **1**, 25–32 (2008).
34. Ricard, Y., Richards, M., Lithgow-Bertelloni, C., & Le Stunff, Y. A geodynamic model of mantle density heterogeneity. *J. Geophys. Res.* **98**, 21895–21909 (1993).
35. Mitrovica, J. X. Haskell [1935] revisited. *J. Geophys. Res.* **101**, 555–569 (1996).
36. Moresi, L., & Solomatov V. Mantle convection with a brittle lithosphere : thoughts on the global tectonic styles of the Earth and Venus. *Geophys. J. Int.* **133**, 669–682 (1998).

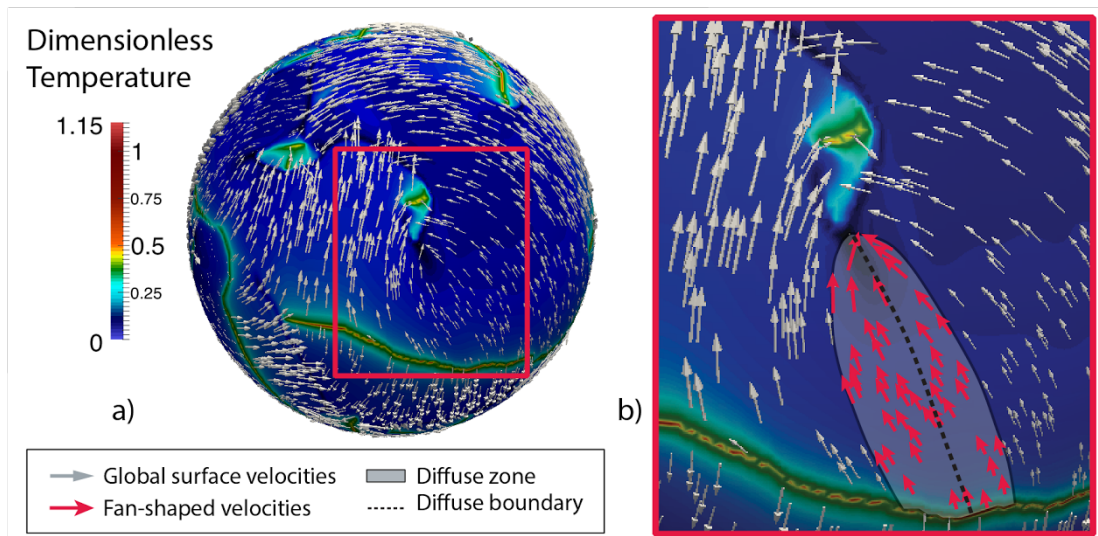


37. Trompert, R. & Hansen U. Mantle convection simulations with rheologies that generate plate-like behaviour. *Nature*. **395**, 686–689 (1998).
38. Tackley, P. J. Self-consistent generation of tectonic plates in time-dependent, three dimensional mantle convection simulations : 1. Pseudoplastic yielding. *Geochemistry, Geophys. Geosystems*. **1** (2000a).
39. Tosi, N., Stein, C., Noack, L., Hüttig, C., Maierová, P., Samuel, H., Davies, D.R., Wilson, C.R., Kramer, S.C., Thieulot, C., Glerum, A., Fraters, M., Spakman, W., Rozel, A. & Tackley, P.J. A community benchmark for viscoplastic thermal convection in a 2-D square box. *Geochem. Geophys. Geosyst.* **16**, 2175–2196 (2015).
40. Van Heck, H. J., & Tackley, P. J. Planforms of self-consistently generated plates in 3D spherical geometry. *Geophys. Res. Lett.* **35**, 19312 (2008).
41. Gordon, R. G. Diffuse Oceanic Plate Boundaries : Strain Rates, Vertically Averaged Rheology, and Comparisons with Narrow Plate Boundaries and Stable Plate Interiors, *History and Dynamics of Global Plate Motions, Geophys. Monogr. Ser.* **121**, 143–159 (2000).
42. Gourdazi M. A., Cocard, M., Santerre. R. EPC : Matlab software to estimate Euler pole parameters. *GPS Solut.* **18**, 153-162 (2014).
43. Zhong, S., Gurnis, M., Moresi, L. Role of faults, nonlinear rheology, and viscosity structure in generating plates from instantaneous mantle flow models, *J. of Geophys. Res.* **103**, 15255-15268 (1998).

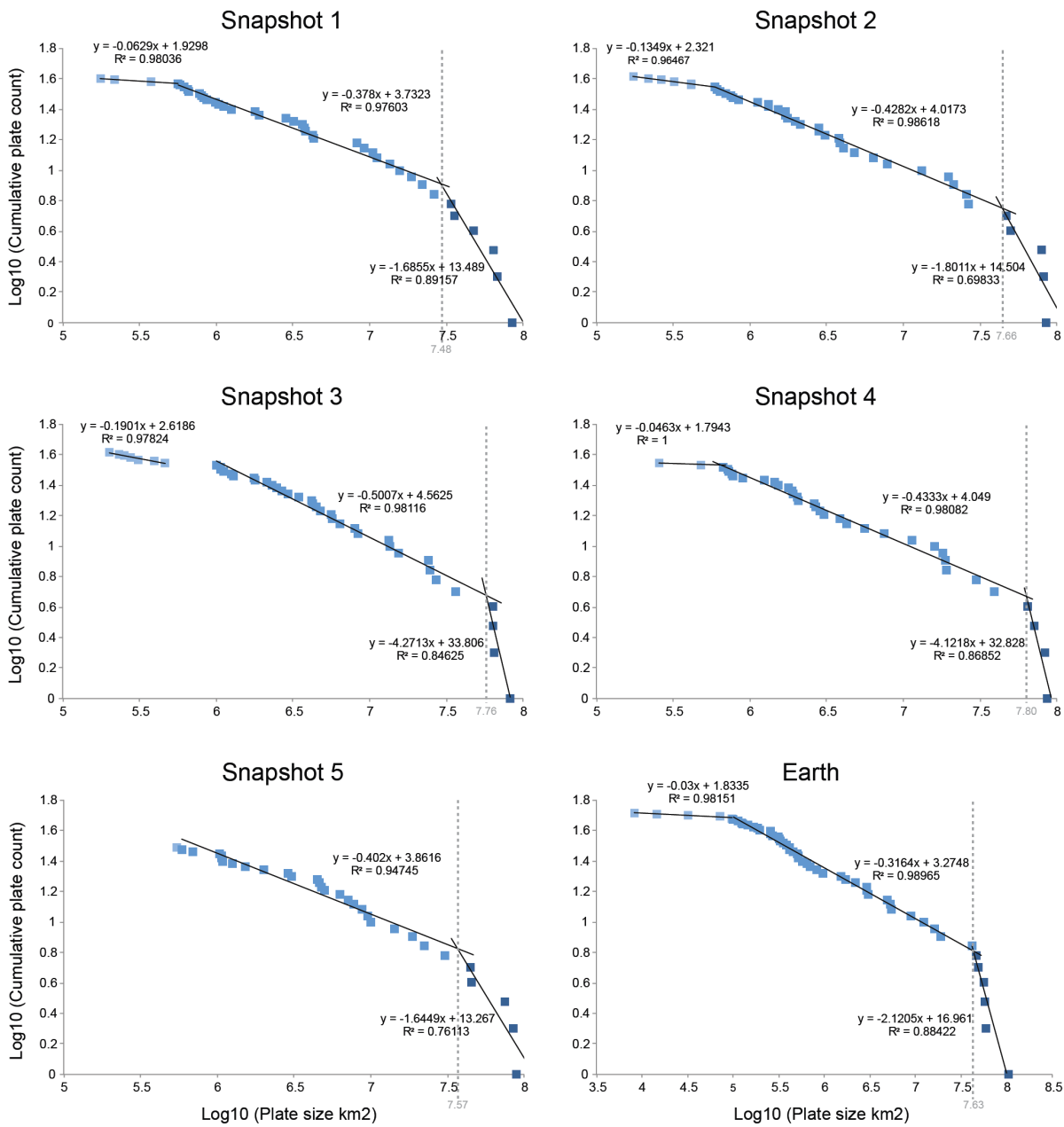
## Extended Data



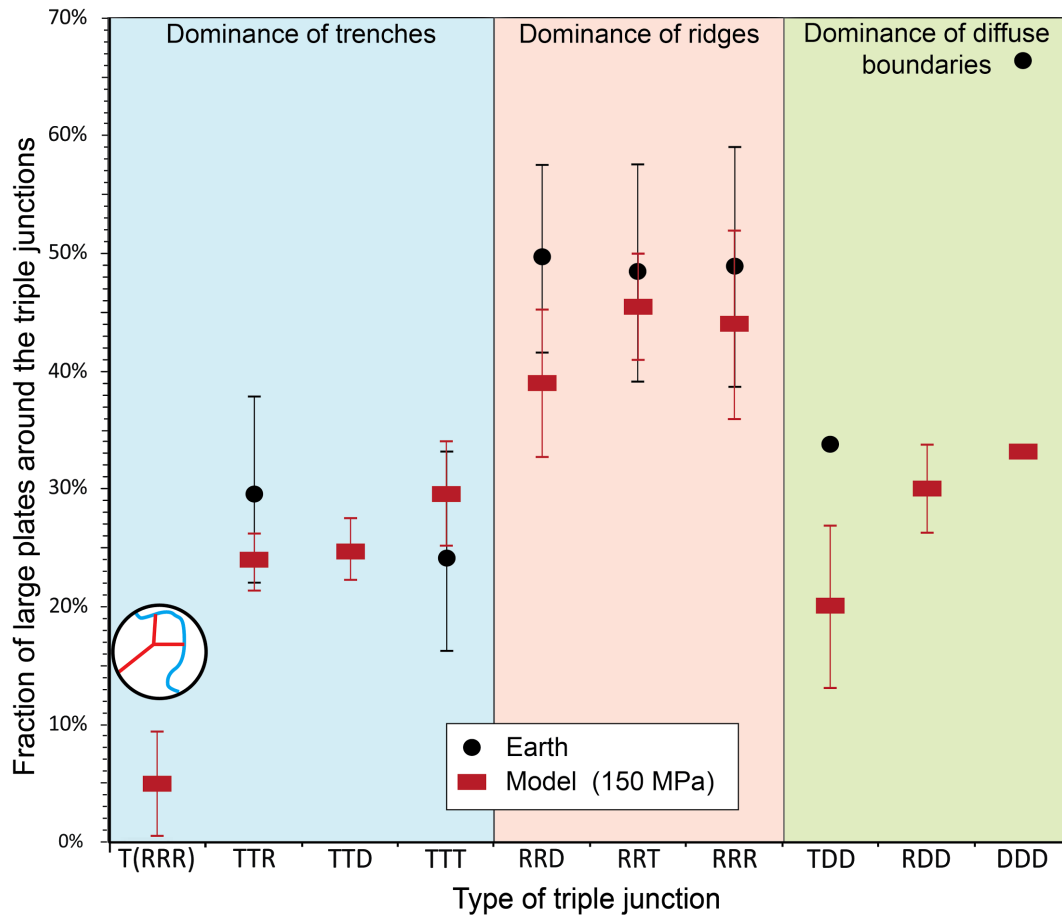
Extended Data Figure 1: Maps of the surface of snapshot from a convection model with a yield stress of 150 MPa and of Earth plate layout. **a.** Map of seafloor age with youngest age in red characteristic of mid-ocean ridges and oldest zones in blue characteristic of subduction zone. **b.** Map of non-dimensional horizontal divergence with divergence zones (mid-ocean ridges) shown in red and convergence zones (subduction zones) in blue. **c.** Map of plate sizes of the convection model and **d.** of the Earth. Plate size categories are determined in Extended Data Fig. 3.



Extended Data Figure 2: Sub-surface temperature of convection models with yield stress 150 MPa. **a.** Global temperature and surface velocities. The dark zones represents subduction zones and the light zones mid ocean ridges. **b.** Zoom of a diffuse boundary: fan of velocities in red characterizes the intra plate diffuse zone allowing the determination of a diffuse boundary.



Extended Data Figure 3: Detail of the Plot of the logarithm of cumulative plate count vs. the logarithm of plate size in km<sup>2</sup> for the fourth snapshots of the model 2 and for the Earth<sup>2</sup>. This graph shows a distribution of microplates in light blue, small plates in intermediate blue and large plates in dark blue. The slopes are calculated in black and the correlation coefficient  $R^2$  too.



Extended Data Figure 4: Plot of the fraction of large plates adjoining a triple junction vs. the type of triple junction for model 2 in red and for the Earth (Bird 2003) in black. The colored backgrounds indicate of dominance of each boundary type: the blue background indicates that the triple junctions are mainly composed by subduction zones, the red background shows a dominance of mid-ocean ridges or transform and a dominance of diffuse boundaries for the green one. T: trenches, R: ridges and D: diffuse boundary. We added a type of triple junction T(RRR): these triple junctions are directly connected to curved trenches and produce back-arc basins with small plates, hence they are part of subduction zones dominance. The error bars represent the standard deviation of the fraction of large plates around a triple junction for the model and the Earth.